

Dynamic Fracture Characterization of Material

A.S. Kobayashi, A.F. Emery, B.M. Liaw

*Department of Mechanical Engineering,
University of Washington, Seattle, Washington 98195, U.S.A.*

In a recent paper, the authors reported on the differences in dynamic fracture responses of three Araldite B fracture specimens with small differences in the dynamic fracture toughness versus crack velocity relations. The influences of a wide range of material properties, i.e. of A533B steel, a silicon nitride ceramic and a Homalite-100 photoelastic polymer, as well as the influences of the specimen sizes on the dynamic fracture response of fracture specimens are presented in this paper. The results of a numerical study show that the dynamic fracture responses of these fracture specimens of proportional dimensions were indistinguishable provided the normalized dynamic fracture toughness versus normalized crack velocity relations of the three materials coincide.

The limited results in this paper as well as in previous papers suggest that should the normalized dynamic fracture toughness versus normalized crack velocity relations between prototype and model materials coincide, then dynamic fracture experiments on scaled models can be used to infer the dynamic fracture response of the prototype.

1. Introduction

Recent research efforts in dynamic fracture characterization of reactor grade steel were aimed toward assessing the crack arrest capability of a reactor vessel subjected to thermal shocking during emergency core cooling (ECC) following a loss of coolant accident (LOCA). Limited thermal shock experiments on scaled thick-walled cylinders [1] have been conducted where the crack run-and-arrest history of one test result was later duplicated with a finite-difference model of the thermally-shocked cylinder using a postulated dynamic fracture toughness versus crack velocity relation [2]. One of the uncertainties involved in such analysis is the postulated dynamic fracture toughness versus crack velocity relation, where direct measurement of these quantities are difficult if not impossible to obtain [3,4]. Using the experimentally more readily accessible photoelastic polymers one of the authors has determined these relations and found excellent agreements between the experimentally and numerically determined dynamic stress intensity factors in dynamically fracturing specimens [5]. The influence of experimentally observed variations in dynamic fracture toughness versus crack velocity relations on the crack propagation histories in these polymer fracture specimens was found to be substantial in larger fracture specimens, while such influence was found to be negligible in smaller specimens [6]. These results, when projected to metal specimens, lead to an intolerable recommendation of testing large metallic fracture specimens if a conservative estimate of the arrest crack length is to be obtained under LOCA/ECC condition. The purpose of this paper is to systematically reanalyze the above scenario in order to delineate the material and size effects on dynamic fracture response of fracture specimens.

2. Fracture Specimens

As idealized materials, a rate-sensitive A533B steel, Homalite-100 photoelastic polymer and a rate insensitive silicon nitride ceramics, Si_3N_4 , were selected as extremes of material properties. The dynamic fracture toughness versus crack velocity relations for A533B steel [7], Homalite-100 [8,9] and additionally, Araldite B photoelastic polymers [10] are shown in Figure 1. No comparable data is available for silicon nitride although preliminary data [11] show that this ideally brittle material is not as rate insensitive as expected. For convenience in numerical analysis the different fracture properties of the known A533B steel and photoelastic polymers and the unknown silicon nitride were combined and identified by the thin solid line shown in Figure 1.

Figure 2 shows the finite element breakdown of a single edge notches (SEN) specimen with three prescribed end loads of uniform load, uniform displacement and linearly varying displacement which were considered in this paper. In addition to the basic SEN specimen shown in Figure 2, the same specimen was scaled ten and hundred times its original geometry for dynamic fracture analysis.

3. Dynamic Fracture Analysis

A dynamic finite element code was executed in its "propagation phase" by propagating the crack according to the idealized and normalized dynamic fracture toughness versus crack velocity relation in Figure 1. Details of this dynamic finite element code and its use in solving dynamic fracture problems are given in Reference [5,6] and therefore will not be repeated here. The procedure used in this propagation analysis is to first load the specimen until the static stress intensity factor, K_I , of the pre-existing edge crack reaches the prescribed fracture toughness, K_{IC} . The crack is then propagated one finite element node at a time following the prescribed nodal release mechanism [5] and the dynamic stress intensity factor

is computed from the energy dissipated at the released crack tip node.

4. SEN Specimen Subjected to Three End Loadings

4.1 Uniform Load

Figure 3 shows the increasing static and dynamic stress intensity factors K_I and K_I^{dyn} , respectively, with crack extension in the A533B steel and Si_3N_4 SEN specimens, subjected to uniform load. The distinct lag in the increase of K_I^{dyn} with respect to K_I resulted in the energy partitions of Figure 4 where the released energy greatly exceeded the fracture energy dissipated by the crack which is propagating at its prescribed terminal velocity of $\dot{a} = 0.15C_1$. The kinetic energy in the specimen continually increases and imparts significant dynamic effects on the small fracture specimen.

Figure 3 also shows that despite the two-fold plus difference in the dilatational wave velocities, C_1 , and the 30-fold difference in the fracture toughness, K_{IC} , the normalized dynamic stress intensity factors, K_I^{dyn}/K_{IC} , of A533B steel and the brittle Si_3N_4 nearly coincide throughout the entire crack propagation history. This coincidence, despite the significant dynamic effects generated by the excessive kinetic energies, is an indication that the normalized K_{ID}/K_{IC} versus \dot{a}/C_1 relation controls the elastodynamic crack propagation.

4.2 Uniform Displacement

The same A533B steel and Si_3N_4 SEN specimens under fixed grip (uniform displacement) loading was also analyzed. The static stress intensity factor, K_I , in Figure 5 reaches a maximum value of about three times the fracture toughness, K_{IC} . The dynamic stress intensity factor, K_I^{dyn} , tends to catch up with the static K_I with crack propagation in these specimens. K_I^{dyn} for both the A533B steel and the Si_3N_4 are more than twice the corresponding K_{IC} values during crack propagation and thus crack arrest will not occur under this loading. Again, the coincidence of K_I^{dyn}/K_{IC} curves of both A533B steel and Si_3N_4 is noted.

The closeness of the static K_I and the dynamic K_I^{dyn} , in contrast to the previous SEN specimens, suggests that the kinetic energy and hence the dynamic effects should not be excessive. Figure 6 shows that while the fracture energy is about the same as that in Figure 4, the kinetic energy is about one fourth of that in Figure 4. The smaller dynamic effects are thus suggested in these specimens.

4.3 Linearly Varying Displacement

Figure 7 shows the dynamic fracture responses of A533B steel and Si_3N_4 SEN specimens subjected to linearly varying displacement loadings. The static K_I after reaching a maximum value of about 1.8 times K_{IC} decreases rapidly and drops below $0.8 K_{IC}$ at about 63 percent of the specimen width. The normalized K_{ID}/K_{IC} versus \dot{a}/C_1 curve in Figure 1 shows that crack arrest is inevitable at this point if the crack is still propagating. It is also noted that K_I^{dyn} in these SEN specimens never attains a large value.

Dynamic fracture analyses of A533B steel and Homalite-100 SEN specimens, of 64 x 256 mm as well as 640 x 2560 mm which is ten times the size of the SEN specimens considered in Figure 7, were also analyzed. The resultant K_I^{dyn}/K_{IC} versus normalized crack length, a/w , relations thus obtained for the regular as well as one hundred time SEN specimens can be superposed on the K_I^{dyn}/K_{IC} curve of Figure 7 with negligible difference. Agreements between the K_I^{dyn}/K_{IC} histories in A533B steel and Homalite-100 in Figures 7 and 8 are remarkable since Homalite-100 whose dilatational wave velocity is about the same as Si_3N_4 has a fracture toughness about 1/385 of that of A533B steel. The results for hundred times SEN specimens are hardly different from that of Figure 8 and thus are not presented in this paper.

Figure 9 shows the normalized energies with crack propagation in the A533B and Homalite-100 SEN of 64 x 256 mm size. As expected, the fracture energies are relatively small and the kinetic energies are very small, indicating the lack of noticeable dynamic effect in these SEN specimens. The small dynamic effect also assures that once the propagating crack arrested after K_I^{dyn} decreased to $0.8 K_{IC}$, the crack will not restart by the kinetic energy fed back into the crack tip.

5. Conclusions

The widely varying dynamic fracture toughness versus crack velocity relations and material properties were found to have negligible influence on the crack propagation history in the small, 6.4 x 25.6 mm, to the large 640 x 2560 mm SEN specimens. The practical significance of these results are that the normalized K_{ID}/K_{IC} versus \dot{a}/C_1 are the governing dynamic fracture properties in these widely varying materials and specimen sizes regardless of their inherent dynamic effects.

6. Discussion

The above conclusion, which obviously is in need of further verification, indicates that model testing can be used to predict the dynamic fracture response of a prototype reactor component provided the normalized K_{ID}/K_{IC} versus \dot{a}/C_1 relations between the model and prototype materials coincide and that scaled geometries are used. Figure 1 shows that the actual K_{ID}/K_{IC} versus \dot{a}/C_1 relations, and not the idealized relations used in this investigation, of A533B steel and Araldite B are in good agreement when the crack is propagating with a driving force K_I^{dyn} larger than the fracture toughness of K_{IC} . From the conclusion arrived in this paper, it is expected that the results of a dynamic fracturing, Araldite B model can be scaled to predict the corresponding fracture response in A533B steel, prototype. Excluded from this scaling is the critical question involving crack arrest where the K_{ID}/K_{IC} versus \dot{a}/C_1 relations for the A533B steel and Araldite B materials differs significantly as shown in Figure 1. For each investigation, a material which models more precisely the knee of the K_{ID}/K_{IC} versus \dot{a}/C_1 relation of A533B steel must be used provided the latter is an accurate representation of the actual dynamic fracture behavior of A533B steel, a question which has not been conclusively answered yet.

7. Acknowledgement

This investigation was supported by NASA Grant NGL 48-002-004 to the Ceramic Engineering Division, University of Washington. The authors express their gratitude to Professor J. I. Mueller, Principal Investigator of Ceramic Material Research for his support during the course of this investigation.

8. References

- [1] CHEVERTON, R. D., ISKANDER, S. K. and BOLT, S. E., "Applicability of LEFM to the Analysis of PWR Vessels under LOCA-ECC Thermal Shock Conditions", NUREG/CR-0107, ORNL/NUREG-40, Oak Ridge National Laboratory, (1978).
- [2] CHEVERTON, R. D., HAHN, G. T., ISKANDER, S. K. and GEHLEN, P. C., "Application of a Crack Arrest to a Thermal Shock Experiment", Crack Arrest Methodology and Applications, edited by G. T. Hahn and M. F. Kanninen, ASTM STP 711, pp. 342-421, (1980).
- [3] KOBAYASHI, T. and DALLY, J.W., "Dynamic Photoelastic Determination of the \dot{a} -K Relation for 4340 Alloy Steel", *ibid loc cit*, pp. 189-210.
- [4] KALTHOFF, J.F., BEINERT, J., WINKLER, S. and KLEIN, W., "Experimental Analysis of Dynamic Effects in Different Crack Arrest Test Specimens", *ibid loc cit*, pp. 109-127.
- [5] KOBAYASHI, A.S., "Dynamic Fracture Analysis by Dynamic Finite Element Method-Generation and Propagation Analysis", Nonlinear and Dynamic Fracture Mechanics, edited by N. Perrine and S. N. Atluri, ASME AMD Vol. 35, pp. 19-36 (1979).
- [6] HODULAK, L., KOBAYASHI, A.S. and EMERY, A.F., "Influences of Dynamic Fracture Toughness on Dynamic Crack Propagation", Engineering Fracture Mechanics, Vol. 13, pp. 85-93, (1980).
- [7] HAHN, G. T., HOAGLAND, R. G. and CHEVERTON, R. D., "Crack Arrest Methodology for Thick Section", a paper presented at the 5th International Conference on Fracture, Cannes, France, March 31, 1981.
- [8] MALL, S., KOBAYASHI, A.S. and URABE, Y., "Dynamic Photoelastic and Dynamic Finite Element Analyses of Dynamic-tear-test Specimens", Experimental Mechanics, Vol. 18, No. 12, pp. 449-456, (Dec. 1978).
- [9] METCALF, J. T. and KOBAYASHI, T., "Comparison of Crack Behavior in Homalite-100 and Araldite B", Crack Arrest Methodology and Applications edited by G. T. Hahn and M. F. Kanninen, ASTM STP 711, pp. 128-145, (1980).
- [10] KALTHOFF, J., BEINERT, J. and WINKLER, S., "Influence of Dynamic Effect on Crack Arrest", Institut fuer Festkoerpermechanik report prepared under EPRI Contract RP 1022-1, IKFM 40412, (1978).
- [11] KOBAYASHI, A.S., EMERY, A. F. and LIAW, B. M., "Dynamic Fracture Toughness of Glass and Silicon Nitride", to be presented at the International Symposium on the Application of Fracture Mechanics Concepts to Ceramic Materials, Penn State University, (July 15-17, 1981).

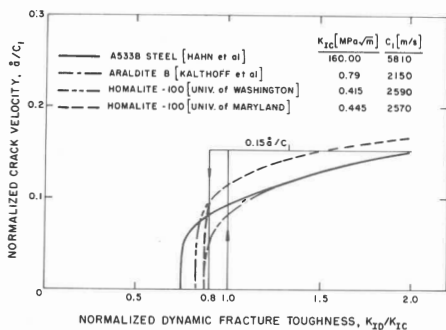


FIG. 1. DYNAMIC FRACTURE TOUGHNESS VERSUS CRACK VELOCITY RELATION.

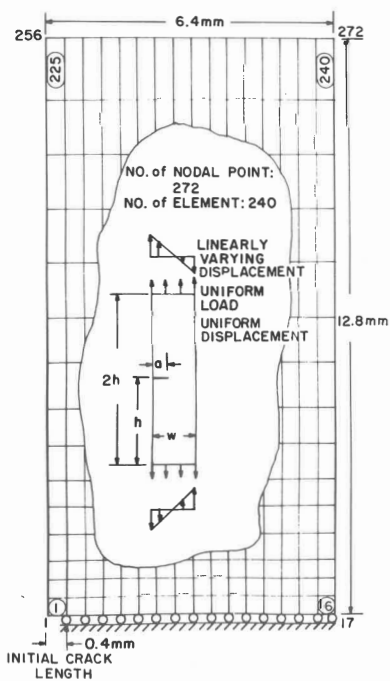


FIG. 2. FINITE ELEMENT BREAKDOWN OF SEN SPECIMEN.

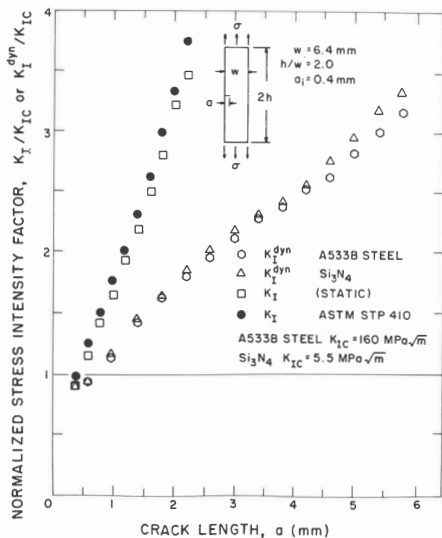


FIG. 3. STRESS INTENSITY FACTOR IN SEN SPECIMEN UNDER UNIFORM LOAD.

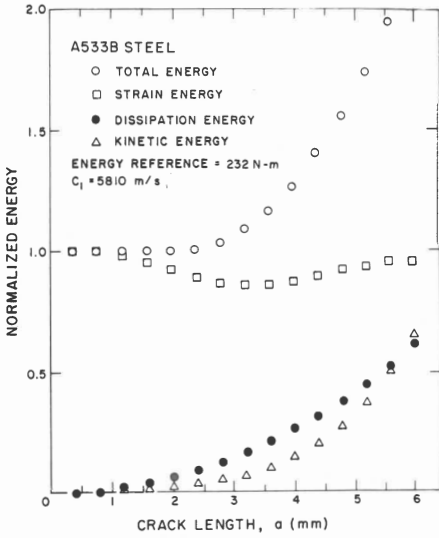


FIG. 4. ENERGIES IN FRACTURING A533B STEEL SEN SPECIMEN UNDER UNIFORM LOAD.

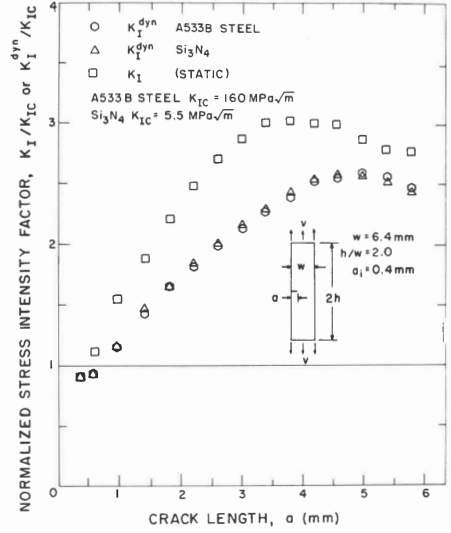


FIG. 5. STRESS INTENSITY FACTORS IN SEN SPECIMEN UNDER UNIFORM DISPLACEMENT LOADING.

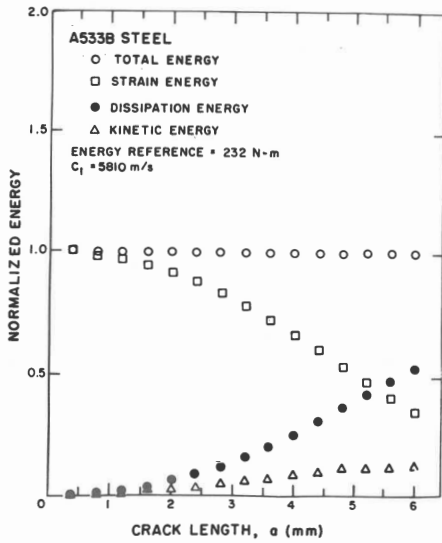


FIG. 6. ENERGIES IN FRACTURING A533B STEEL SEN SPECIMEN UNDER UNIFORM DISPLACEMENT LOADING.

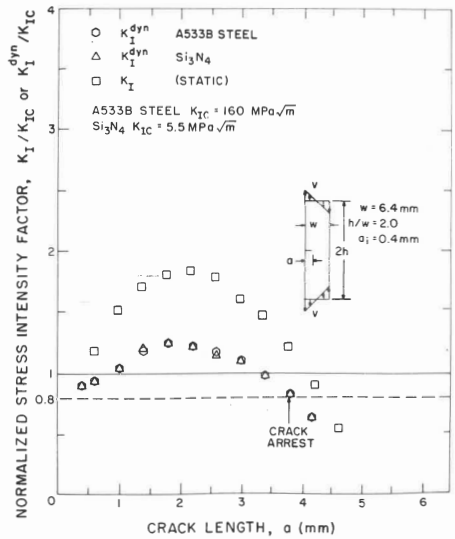


FIG. 7. STRESS INTENSITY FACTORS IN SEN SPECIMEN UNDER LINEARLY VARYING DISPLACEMENT LOADING.

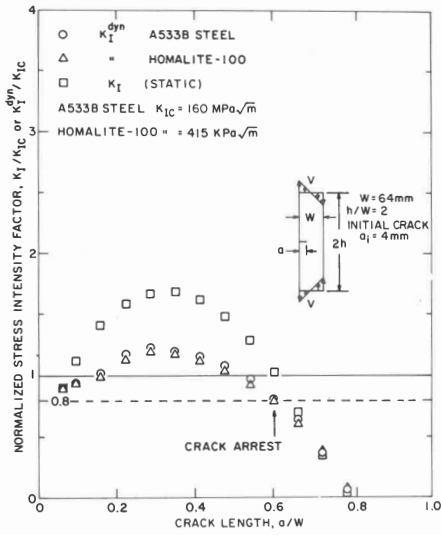


FIG. 8. STRESS INTENSITY FACTOR IN NOTCHED BEND SPECIMENS WITH LINEARLY VARYING DISPLACEMENT LOADING.

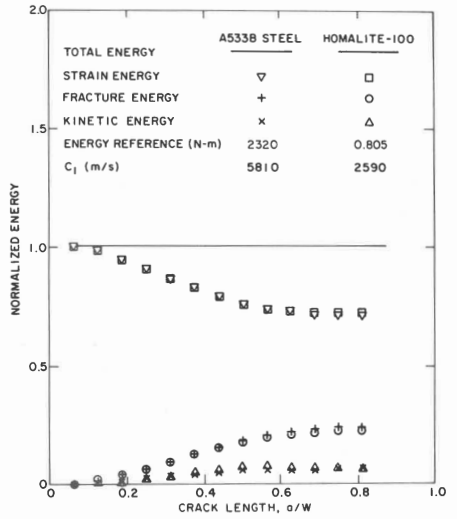


FIG. 9. ENERGY PARTITION IN NOTCH BEND SPECIMEN WITH LINEARLY VARYING DISPLACEMENT LOADING.